

MIXING AND REFINING DYNAMICS OF A GAS STIRRED THREE-PHASE REACTOR BY CFD ANALYSIS

Jan Erik OLSEN, Harald LAUX and Joakim B OIAN

SINTEF Materials and Chemistry, 7465 TRONDHEIM, NORWAY

ABSTRACT

A multi-fluid model for gas stirred gas/liquid/liquid reactors with mass transfer between the two liquid phases has been developed within a commercial CFD code. Using the CFD model a scale up study of a gas/metal/slag reactor in which an unwanted impurity element is transferred from the metal to the slag phase has been carried out. Reactors of two different sizes and with four different gas-stirring rates have been simulated. The results show that scale up of the smaller reactor increases the metal productivity significantly, and that the refining rate increases significantly with increasing gas rate.

INTRODUCTION

Gas-stirred reactors with two liquids are applied in refining processes where the purpose of the process is to mix the liquids well and facilitate fast transfer of impurities from one liquid to the other. Due to process conditions such as possible high temperatures and non-transparent liquids, it is often difficult to study the process in detail. Mathematical models describing the underlying physics may thus be helpful in understanding the local and global behavior of the process. In particular, they may serve as a tool for optimizing the reactor design and process conditions.

In order to quantitatively describe the refining process a mathematical model has been developed. Due to the complexity of the system, the model is not expected to predict results quantitatively accurate. Still the quantitative predictability is reasonable as shown below. The model will predict the qualitative behavior of the system, and the relative comparison between simulations with different parameter settings is expected to be very accurate. The model is thus applicable to analysis regarding process optimization and reactor design. In the following sections the model is presented and applied to a study on the scale up of a reactor with respect to gas rate optimization. Reactors may be designed in different shapes and with different types of gas inlets. We will focus on box shaped reactors with a bottom inlet for gas bubbles. The impurities are present in small concentrations, but the specification of the final product quality demands an even higher degree of purity.

MATHEMATICAL MODEL

To describe the mixing and refining dynamics of gas stirred reactors, a mathematical model has been developed within the framework of the CFD code Fluent (2005). The reactor is assumed to contain two liquids being mixed with the purpose of altering the composition of the liquids. Each liquid is a mixture of a solvent and different species present in small concentrations. Mixing of the liquids is driven by inert gas bubbles injected into the reactor. The gas injected into the reactor tends to accumulate at the top of the reactor where it acts as a cover gas. It is assumed that the reactor is well isolated such that near isothermal conditions prevail.

The mathematical model consist of an Eulerian multi-fluid model for the liquids and the cover gas. The gas bubbles are accounted for by a Lagrangian model interacting with the Eulerian phases through drag forces. The Eulerian phases also impose turbulent dispersion on the Lagrangian bubbles. Reasons for applying a mixed Eulerian/Lagrangian approach is given below. The dynamics of this mixing process is significantly affected by the size of the gas bubbles and the size of the liquid droplets. A model for bubble and droplet sizes is therefore necessary to describe the mixing dynamics properly. Droplet sizes are also important for the refining rate. Refining is accounted for by mass transfer of species between the liquid phases. The mathematical model presented below is later on applied to a three-phase reactor, but it will also be applicable to systems with more than three phases.

Eulerian Model

The fluid flow of the two liquids and the cover gas in the three-phase reactor is modeled by an Eulerian multi-fluid model (T B Anderson and R Jackson, 1967). We solve for conservation of mass and momentum for each phase.

The continuity equation for phase q is

$$\frac{\partial}{\partial t} (\alpha_q \rho_q) + \nabla \cdot (\alpha_q \rho_q \vec{v}_q) = 0 \quad (1)$$

where α_q , ρ_q and \vec{v}_q are the volume fraction, physical density and velocity of phase q respectively. In the phase mass conservation equations, mass transfer of species is neglected since the concentration of the impurity element is assumed never to exceed a few hundred ppmw.

The momentum equation for phase q is

$$\frac{\partial}{\partial t} (\alpha_q \rho_q \vec{v}_q) + \nabla \cdot (\alpha_q \rho_q \vec{v}_q \vec{v}_q) = -\alpha_q \nabla p + \nabla \cdot \bar{\tau}_q + \alpha_q \rho_q \vec{g} + \sum_{l=1}^n \vec{R}_{lq} + \vec{F}_p \quad (2)$$

where $\bar{\tau}_q$ is the q^{th} phase stress tensor which for a Newtonian fluid is

$$\bar{\tau}_q = \alpha_q \mu_q (\nabla \vec{v}_q + \nabla \vec{v}_q^T) - \frac{2}{3} \alpha_q \mu_q \nabla \cdot \vec{v}_q \bar{I} \quad (3)$$

Here μ_q is the effective shear viscosity of phase q , p is the pressure shared by all phases, \vec{R}_{lq} is an interaction force between phase q and l , and \vec{F}_p is the interaction force from the gas bubbles accounted for by a discrete particle model. Turbulence is modeled by solving transport equations for turbulent kinetic energy and dissipation rate for each phase (i.e. k- ϵ model based on Launder and Spalding (1974)).

The Eulerian phases are assumed to consist of a continuous phase and one or more dispersed phases. For these kinds of bubbly mixtures, the interaction force between the phases may be modeled by the following expression:

$$\vec{R}_{lq} = \frac{(\alpha_q \rho_q + \alpha_l \rho_l) \alpha_l f}{\tau_{lq}} (\vec{v}_l - \vec{v}_q) \quad (4)$$

where τ_{lq} is the *particulate relaxation time*

$$\tau_{lq} = \frac{(\alpha_l \rho_l + \alpha_q \rho_q) \left(\frac{d_q + d_l}{2} \right)^2}{18 (\alpha_l \mu_l + \alpha_q \mu_q)} \quad (5)$$

and f is the *drag function*

$$f = \frac{C_D \text{Re}}{24} \quad (6)$$

Here C_D and Re are the drag coefficient and Reynolds number as defined by Schiller and Naumann (1935), and d_q and d_l are particulate sizes of the two phases interacting. Note that turbulent dispersion is not accounted for.

Since both the drag function and the particulate relaxation time depend significantly upon bubble and/or droplet size, the interphase interaction is strongly influenced by bubble and/or droplet size. Thus it is important to implement a good description of the average bubble and droplet size. A model for average bubble and droplet sizes is described below.

Lagrangian bubbles

Gas bubbles injected at the bottom inlet are accounted for by a Lagrangian discrete particle model (Crowe et al., 1998). The model predicts translational motion of particles from Newton's second law. Bubbles are assumed to be spherical particles, although a shape factor may be implemented to describe motion of non-spherical particles. Newton's law gives the following equation for the velocity of the bubbles

$$m_p \frac{d\vec{u}_p}{dt} = \vec{F}_D + \frac{\vec{g}(\rho_p - \rho)}{\rho_p} \quad (7)$$

where m_p , \vec{u}_p and ρ_p are the mass, velocity and density of the bubbles, ρ is the fluid density, \vec{g} is the gravitational force and \vec{F}_D is the drag force. Turbulent dispersion of bubbles is modeled by a stochastic discrete-particle approach

known as the *discrete random walk model* (Fluent, 2005). The applied drag force accounts for hindered settling, and is written in the following form

$$\vec{F}_D = \frac{\vec{F}_{SN}}{(1 - \alpha_p)^{5.1}} \quad (8)$$

Here \vec{F}_{SN} is the drag force of Schiller and Naumann (1935) and α_p is the volume fraction of the gas bubbles.

The momentum transfer from the Lagrangian bubbles to the continuous phase is computed as

$$\vec{F}_p = \sum \left(\frac{18\mu C_D \text{Re}}{24\rho_p d_p^2} (\vec{u}_p - \vec{u}) \right) \dot{m}_p \Delta t \quad (9)$$

where μ is the viscosity of the fluid, Re is particle Reynolds number, u is fluid velocity, C_D is drag coefficient, \dot{m}_p is mass flow rate of bubbles, and Δt is the time step.

Bubble and Droplet Size

As mentioned above the size of bubbles and droplets significantly affect the dynamics of the reactor. The local average size \bar{d} of bubbles and droplets in the Eulerian phases is described by the following transport equation (Laux and Johansen, 1999):

$$\frac{\partial \bar{d}}{\partial t} + \nabla \cdot (\alpha_d \rho_d \bar{v} \bar{d} - D_{eff} \nabla \bar{d}) = \alpha_d \rho_d \frac{d_{eq} - \bar{d}}{\tau_{rel}} \quad (10)$$

Here D_{eff} is the effective dispersion coefficient, τ_{rel} is the relaxation time, and d_{eq} is the equilibrium diameter. The equilibrium diameter for bubbles and droplets in a turbulent flow is given by (Calderbank, 1958)

$$d_{eq} = C_1 \alpha_d^{0.5} \frac{(\sigma/\rho)^{0.6}}{\epsilon^{0.4}} \left(\frac{\mu_d}{\mu} \right)^{0.25} + C_2 \quad (11)$$

where α_d is the volume fraction of the dispersed phase being considered (i.e. either local bubble or droplet volume fraction), σ is the surface tension, ρ is the density of the continuous phase, μ_d and μ are the viscosities of the dispersed phase and the continuous phase, and ϵ is the turbulent dissipation rate of the dispersed phase. The coefficients C_1 and C_2 are given by empirical data. Note that Calderbank's relation was established for a system with only one dispersed phase. Still we have chosen to apply it to a system with multiple dispersed phases due to the lack of a more general relation.

Equation (10), which is based upon an Eulerian description, needs to be modified to be applicable to the gas bubbles, since the gas bubbles injected at the bottom are accounted for by a Lagrangian method. The Lagrangian version of Eq.(10) is given by

$$\frac{d\bar{d}}{dt} = \alpha_d \rho_d \frac{d_{eq} - \bar{d}}{\tau_{rel}} \quad (12)$$

where diffusion has been neglected. The equilibrium size d_{eq} is given by Eq.(11) with ϵ being the turbulent dissipation rate of the continuous phase. Coefficients C_1 and C_2 will not be equal to the coefficients of the Eulerian bubbles and/or droplets.

Refining Model

The species conservation equation in an Eulerian frame of reference is given by the following equation:

$$\frac{\partial}{\partial t}(\rho_q \alpha_q C_{i^q}) + \nabla \cdot (\rho_q \alpha_q \vec{v}_q C_{i^q}) = -\nabla \cdot \alpha_q \vec{N}_{i^q} + \dot{M}_{i^q} \quad (13)$$

where ρ_q , α_q and \vec{v}_q are density, volume fraction and velocity of phase q , C_{i^q} is mass fraction of species i in phase q , \dot{M}_{i^q} is mass transfer of species i to phase q , and \vec{N}_{i^q} is diffusion of species i due to concentration gradients in phase q

$$\vec{N}_{i^q} = -\rho_q D_{i^q} \nabla C_{i^q} \quad (14)$$

Here, D_{i^q} is the diffusion coefficient for species i in the phase q .

The mass transfer rate for a species i in phase q is

$$\dot{M}_{i^q} = \sum_p A_{pq} J_{i^q j^p} \quad (15)$$

where A_{pq} is the interfacial area density between phase p and q and $J_{i^q j^p}$ is the mass flux of species i from phase q to species j in phase p . The exact description of the mass flux depends upon the nature of the refining physics. For typical absorption processes or processes involving infinite chemical reaction rates at the droplet interface we may derive the following equation for the mass flux (Deo and Boom, 1993):

$$J_{i^q j^p} = \frac{(L * C_{j^p} - C_{i^q})}{1/\rho_q k_{j^p} + L/\rho_p k_{j^p}} \quad (16)$$

where L is the concentration ratio of the species in phase p and phase q at equilibrium, k_{j^q} is the mass transfer coefficient of species i in phase q and k_{j^p} is the mass transfer coefficient of species j in phase p . The mass transfer coefficient is given by the Sherwood number for spherical particles (Bird et al., 1960). The interfacial area density A_{pq} is a function of the droplet size d and the dispersed phase volume fraction α_d

$$A_{pq} = \frac{6\alpha_d}{d} \quad (17)$$

Note that this only describes mass transfer at the interfaces between dispersed particulates and suspending fluid.

Boundary and Initial Conditions

Most boundaries in a geometry are treated as walls with *no-slip* condition for the fluid phases and reflective condition

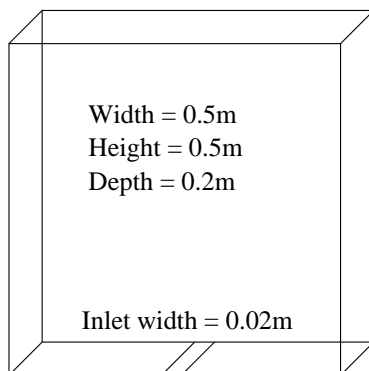


Figure 1: Box-shaped reactor with porous plug for gas injection.

for the gas bubbles. Walls at the top of the geometry will allow gas bubbles to be ejected. Inlets are also treated as walls with the exception of a specified source of gas bubbles given as mass flow rate. If gas bubbles enter a region of pure gas, they are absorbed into the Eulerian gas phase (i.e. removed from the calculations).

Depending upon process conditions, different initial conditions may be studied. Here we assume that the fluids are at rest with a slag layer at the bottom, a metal layer above and gas at the top. Gas bubbles are introduced through a bottom inlet or a lance at the start of the process.

Implementation and Validation

The mathematical model described above is implemented in Fluent 6.2 with user defined functions and user defined scalars for bubble and droplet size, hindered settling, absorption of gas bubbles into the cover gas and mass transfer sources. Note that the turbulent dispersion model in Fluent 6.2's Eulerian multi-fluid model tends to generate stability problems in the presence of large scale interfaces, i.e. interfaces that separate continuous fluid layers. The gas bubbles, however, are significantly affected by turbulent dispersion and their distribution in turn strongly affects the flow pattern. This forces us to model the bubble phase in a Lagrangian manner and to leave out the effect of turbulent dispersion on the Eulerian droplets.

The model has been calibrated and validated against experiments in a transparent water-oil-air reactor. Water, silicone oil and air was used in a mixing experiment in a box-shaped glass tank illustrated in Fig.1. Gas bubbles were injected through a porous plug in the bottom of the reactor. The coefficients in the bubble and droplet size models were calibrated resulting in the values $C_1 = 0.37$ and $C_2 = 100\mu\text{m}$ for the Lagrangian bubbles and $C_1 = 2.0$ and $C_2 = 100\mu\text{m}$ for the Eulerian droplets (Olsen et al., 2007).

Refining experiments were carried out in a commercial gas stirred slag-metal reactor with gas injected through a lance. In Fig.2 we see the refining progress of an impurity in the metal phase. Results from the CFD model presented above are compared to experimental results and results from a point model. The point model assumes perfect mixing above the lance inlet and no mixing below. We see from Fig.2 that the CFD model is capable of describing realistic refining processes with reasonable accuracy for engineering purposes. Due to confidentiality further details of the experiment can not be released.

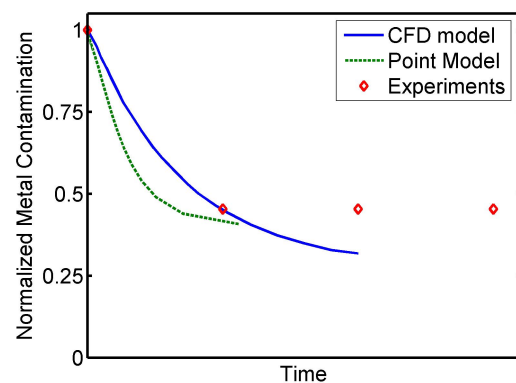


Figure 2: Normalized impurity concentration as function of time.

Table 1 Normalized material properties at process conditions.

ρ_{slag}	1.07
ρ_{metal}	1
ρ_{gas}	$7.72 \cdot 10^{-5}$
μ_{slag}	259.01
μ_{metal}	1
μ_{gas}	0.02
$\sigma_{gas/slag}$	0.54
$\sigma_{gas/metal}$	1
$\sigma_{metal/slag}$	0.86
L	3
D_{slag}	0.15
D_{metal}	1

ANALYSIS OF REACTOR SCALE UP

Numerical calculations have been carried out to study the effect of gas rate and scale up upon the mixing and refining dynamics of a gas-metal-slag reactor with material properties at the system temperature as given in Table 1. The reactor has a volume of 50 l and is similar to the box shaped reactor described above with the exception of its content. Initially the reactor is filled with 40% slag at the bottom, 40% metal in the middle and 20% gas at the top. The metal contains 100 ppmw of a given impurity. Based on empirical observations it is assumed that slag is the continuous phase. The numerical calculations have been carried out on a two-dimensional mesh of 10000 cells (i.e. 5mm resolution) with a timestep of 0.0002 sec. The Fluent solver uses a SIMPLE-based time-stepping algorithm (Patankar, 1980) and allows the user to choose between different spatial (convective terms) and temporal discretization schemes. We have used first order accurate schemes for turbulence and species transport equations and higher order schemes for velocity and mass conservation equations. For discretization in time a second order implicit scheme was applied. The calculations were carried out until the contamination level declined to 27 ppmw (25 ppmw being the equilibrium concentration). Typical CPU times were about 3 weeks on a single CPU node.

The effect of gas rates has been studied by running several calculations for relatively high gas rates varying between 330 l/min and 1200 l/min in the reactor of 50 l. In the beginning the gas bubbles rise from the bottom inlet. Due to turbulent dispersion the bubble plume spreads outwards as shown in Fig.3. The gas bubbles transfer momentum to the slag phase and lift the slag upwards and into the metal phase. This is seen in Fig.4 for a gas rate of 660 l/min. As slag reaches the gas phase it is pushed out towards the sidewalls before it drops towards the bottom again (see Fig.5). This creates a circulating motion of the liquids which again influences the motion of the gas bubbles. The gas bubbles are pushed sideways by the liquid motion as the slag returns to the lower parts of the reactor. Depending on gas rate, good mixing is achieved after a start up time of typically 20-60 sec.

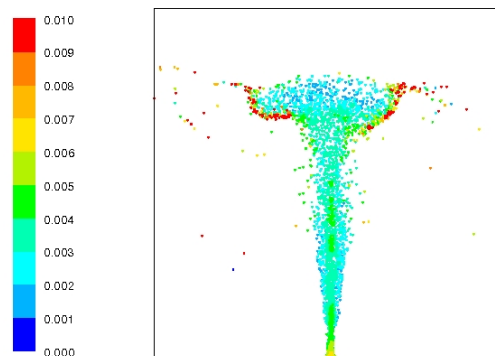


Figure 3: Gas bubble distribution colored by bubble size (m) after 2 seconds of process time.

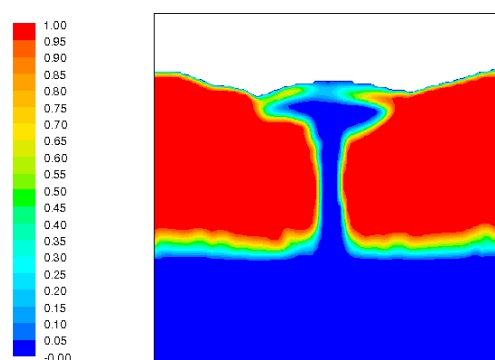


Figure 4: Volume fraction of metal after 2 seconds of process time.

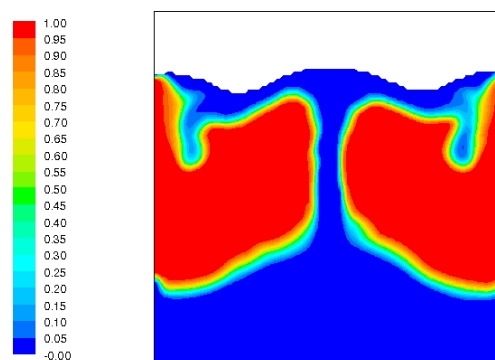


Figure 5: Volume fraction of metal after 5 seconds of process time.

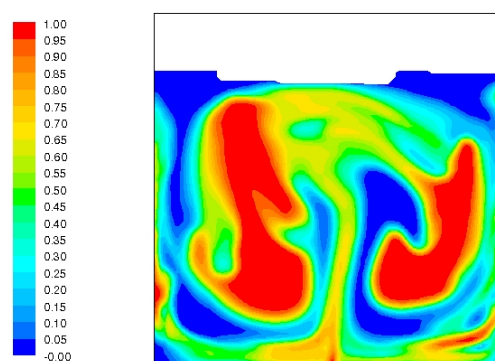


Figure 6: Volume fraction of well mixed metal after 30 seconds of process time.

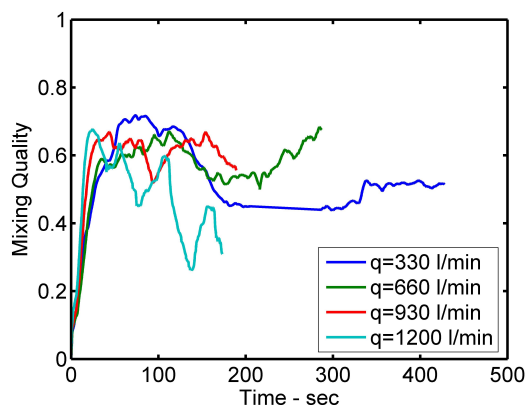


Figure 7: Mixing curves for small reactor (50 l).

This can be seen in Fig.6 where the liquids are well mixed. As metal and slag are mixed more and more, the interfacial area increases and the refining rate increases. The observations mentioned above are more properly illustrated by the enclosed animations.

The reactor performance is judged on refining rates and mixing dynamics. To quantitatively describe the mixing of slag and metal, we define the *mixing quality* as

$$e_m = \frac{4}{V_{liquids}} \int \alpha_{metal} \alpha_{slag} dV \quad (18)$$

The mixing quality has a maximum value of 1 for *perfect mixing*. In Fig.7 we see the development of mixing quality with time for different kinds of gas rates. The mixing quality increases from 0 to a value between 0.6 and 0.8 during a start up time between 20 and 60 seconds. After start up the value of the mixing quality reaches a quasi static value. Higher gas rates yield a shorter start up period, but the quasi static value is not heavily dependent upon the gas rate. Refining rates increase significantly with increasing gas rate. This is illustrated by Fig.8. This cannot be explained by differences in mixing quality which are

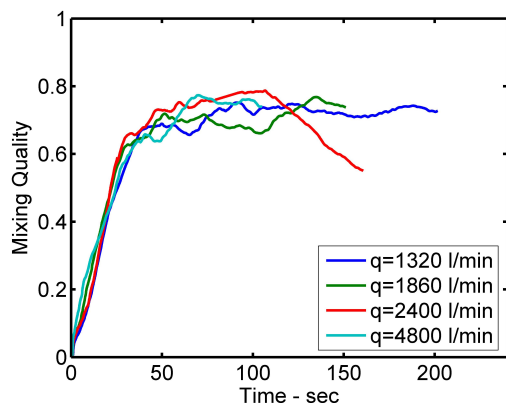


Figure 9: Mixing curves for large reactor (200 l)

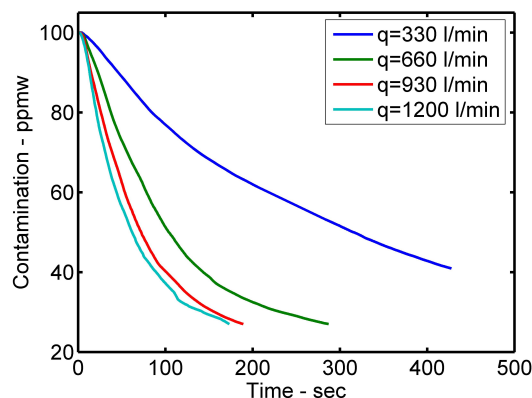


Figure 8: Refining curves for small reactor (50 l).

quite small, but has to be explained by the differences in droplet size and interfacial area as seen in Table 2.

Simulations on a scaled up version of the reactor have also been run to investigate the effect of the scale up on mixing and refining dynamics. The 50 l reactor above was scaled up to a 200 l reactor with dimensions 1m x 1m x 0.2m. Its geometry was meshed with the same resolution as above which yielded a mesh of 40000 cells. Due to the increase in reactor size, it was assumed that the gas rates also needed an increase for the reactor dynamics to be comparable to the dynamics of the smaller reactor. Gas rates between 1320 l/min and 4800 l/min were studied. The mixing quality and the refining curves in Figs.9 and 10 show that the dynamics of the larger reactor is qualitatively quite similar to the smaller reactor. The refining is however faster. The faster refining rate can be explained by better mixing quality as seen when comparing Figs.7 and 9, but it is more likely to be explained by the smaller droplet sizes in the large reactor as seen in Table 2.

When scaling the gas rates accordingly to the scaling of the reactor one might believe that the resulting dynamics remains relatively equal for the original and scaled up reactor. However, the droplet size is a

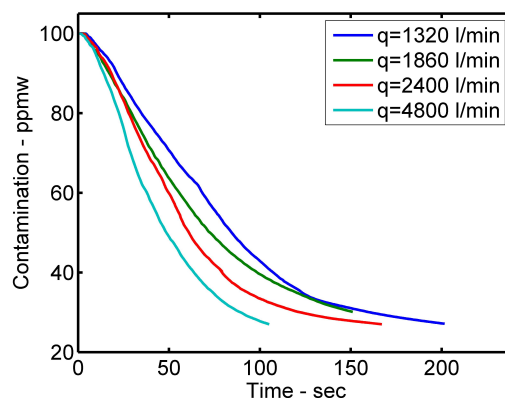


Figure 10: Refining curves for large reactor (200 l).

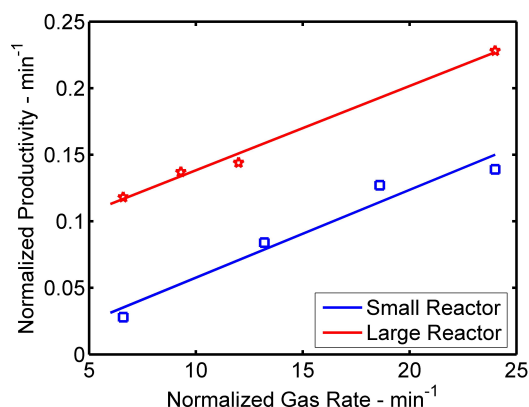


Figure 11: Relative productivity of metal as a function of relative gas rate (i.e. normalized with reactor volume).

function of turbulent dissipation, and turbulence does not necessarily scale with reactor size. Turbulence depends upon absolute gas rates and not relative gas rates. As a result the relative productivity (i.e. productivity normalized with reactor volume) is greater for the large reactor as seen in Fig.11. With productivity we understand the production of metal given as liters per minute. In real production, operating

costs due to labor and maintenance will make the economics of the scaled up reactor even more profitable.

It should be mentioned that we have not considered whether it is possible in reality to scale the gas rate equally with the reactor size. In reality there is an upper limit to how much gas we can put into the reactor. This is limited by such phenomena as gas hold up, possible pressure increase and reactor vibrations. These phenomena do not necessarily scale with reactor size. Thus we can not increase the gas rate indefinitely to increase the productivity.

CONCLUSIONS

A mathematical model for multiphase reactors has been presented. It has been applied to a gas stirred metal-slag reactor. The results show that interfacial area and thus refining rate increases as mixing is improved when gas is injected in the reactor. The refining rate increases with the gas rate. A scale up of the reactor from 50 l to 200 l has a major positive influence on the productivity of the reactor provided that the gas rate may be scaled up accordingly. Limitations on gas rates have not been considered.

REFERENCES

- LAUNDER,B.E. & SPALDING,D.B. *Comput.Meth. Appl.Mech.Eng.*, 3:269, 1974.
- BIRD,R.B., STEWART,W.E. & LIGHTFOOT E.N. *Transport Phenomena*. John Wiley & sons, 1960.
- CALDERBANK. The interfacial area in gas-liquid contacting with mechanical agitation. In *Physical rate processes in industrial fermentation Part I*, volume 36 of *Trans.Instn.Chem.Engrs*, page 443, 1958.
- CROWE,C., SOMMERFELT,M. & TSUJI,Y. *Multiphase flows with droplets and particles*. CRC Press, Boca Raton, Florida, 1998.
- DEO,B. & BOOM,R.. *Fundamentals of steelmaking metallurgy*, pages 124–130. Prentice Hall International, 1 edition, 1993.
- Fluent 6.2 User's Guide*. Fluent Inc., 2005.
- LAUX,H. & JOHANSEN,S.T. A CFD analysis of the air entrainment rate due to a plunging jet combining mathematical models for dispersed and separated multiphase flows. *Fluid Flow Phenomena in Metals Processing, Annual TMS meeting, San Diego*, pages 21–30, 1999.
- OLSEN,J.E., LAUX,H. & ØIAN,J.B. Modeling concepts of a gas stirred liquid-liquid reactor. Abstract submitted to ICMF 2007, Leipzig.
- PATANKAR,S.V. *Numerical Heat Transfer and Fluid Flow*. Taylor & Francis, 1 edition, 1980.
- SCHILLER,N. & NAUMANN,Z. *Z.Ver.Deutsch.Ing.*, 77:318, 1935.
- ANDERSON,T.B. & JACKSON,R. A fluid mechanical description of fluidized beds - equations of motion I. *EC Fundamentals*, 6:527–539, 1967.

Table 2 Global results from reactor calculations

Reactor size and gas rate	Droplet size ¹ \bar{d}_d [mm]	Interfacial area ¹ $\int A dV$ [m ²]	Refining time T_{ref} [sec]	Productivity ² [l min ⁻¹]	Rel.prod. ³ [min ⁻¹]
Small, $\dot{q} = 330$ l min ⁻¹	7.39	10.6	860.0 ⁴	1.40	0.028
Small, $\dot{q} = 660$ l min ⁻¹	5.92	17.8	287.0	4.18	0.084
Small, $\dot{q} = 930$ l min ⁻¹	5.00	21.3	189.2	6.34	0.127
Small, $\dot{q} = 1200$ l min ⁻¹	4.66	22.5	173.2	6.93	0.139
Large, $\dot{q} = 1320$ l min ⁻¹	5.55	77.1	203.8	23.55	0.118
Large, $\dot{q} = 1860$ l min ⁻¹	4.83	90.2	175.5 ⁵	27.35	0.137
Large, $\dot{q} = 2400$ l min ⁻¹	4.55	99.1	167.0	28.74	0.144
Large, $\dot{q} = 4800$ l min ⁻¹	3.59	127.6	105.1	45.50	0.228

1) Value is a time average of values after start up 2) Productivity is amount of metal (liters) divided by refining time (minutes)

3) Relative productivity is productivity per reactor volume 4) Interpolated value from results up to 389 secs.

5) Interpolated value from results up to 133 secs.